Int. J. Solids Structures Vol. 29, No. 7, pp. 893–909, 1992
Printed in Great Britain.

0020–7683/92 $5.00 + .00


# ELASTIC BUCKLING PHENOMENON APPLICABLE TO DEPLOYABLE RINGS

YOSHIAKI GOTO, YASUHITO WATANABE, TOSHIHIRO KASUGAI and MAKOTO OBATA
Department of Civil Engineering, Nagoya Institute of Technology, Gokiso-cho, Showa-ku, Nagoya 466, Japan

(*Received* 30 *August* 1990; *in revised form* 25 *July* 1991)

**Abstract**—There are various kinds of deployable members developed in order to improve the packing efficiency of space structures. Some of them ingeniously utilize elastic buckling phenomena, such as flexural buckling and torsional buckling. However, their application is primarily restricted to straight members. Herein, we present an interesting buckling phenomenon of a ring which considerably reduces its original volume and could be applied to a deployable ring. First, we show an accurate method which can be used to analyze this buckling phenomenon accompanying finite rotations in space. Then, with this method, we theoretically examine the effect of structural parameters on buckling behavior.

## 1. INTRODUCTION

Various kinds of deployable members have recently been developed in order to improve the packing efficiency of space structures. In some of the members, elastic buckling phenomena like flexural buckling and torsional buckling are ingeniously utilized (Natori and Miura, 1985). However, their utilization is primarily restricted to one-dimensional straight members, such as columns and beams.

Herein, we present and theoretically investigate an interesting buckling phenomenon of a ring which considerably reduces its original volume and could be applied to a deployable ring. This buckling phenomenon, classified as a *limit-load instability*, occurs when the external moments shown in Fig. 1 are applied to a ring whose in-plane bending rigidity is smaller than the out-of-plane rigidity. At the locations of the applied moments, the ring is supported such that it is free to move and to rotate only along and around its diameter. As can be seen from the buckling process illustrated in Fig. 2, the ring deforms accompanying considerably large rotations in three-dimensional space and is finally transformed to a small ring with a diameter of one-third of its original size. It is of interest that this final shape is kept without any external force. To our best knowledge, this buckling phenomenon has never even been examined theoretically.

In order to investigate the above buckling phenomenon of a ring theoretically, we have to use an accurate method of analysis which precisely takes into account the geometric nonlinearity, since this buckling behavior accompanies very large rotations in space. The analysis of this kind has been studied by various authors: Love (1944), Antman (1972, 1974), Bathe and Bolourchi (1979), Rankin and Brogan (1984), Simo (1985) and Simo and Vu-Quoc (1986), among others. We have also developed an accurate numerical method which can be applied to the present buckling analysis (Goto *et al.*, 1988). Our method using the *transfer matrix technique* [see Kersten (1962), Pestel and Leckie (1963) and Livesley (1964)] is characterized by the point that the field transfer equations are directly derived from the rigorous governing differential equations of non-linear space rods with Lagrangian

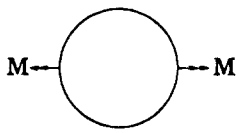


Fig. 1. External moments applied to a deployable ring.

expressions (Goto *et al.*, 1985), different from the method using conventional small-displacement theory within a co-rotational framework. Here, we further improve our method by employing the *incremental arc-length method* (Riks, 1979) such that it can be used to analyze the behavior of limit-load instability accurately.

## 2. DEPLOYABLE RING MODEL

For the analysis of the transformation process of the deployable ring, we here introduce a structural model, as shown in Fig. 3. This ring has a constant doubly symmetric cross-section. A global Cartesian coordinate system $(X, Y, Z)$ is introduced at the initial configuration of the ring with $Z$ along the tangent of the centroidal line. Coordinate axes $(X, Y)$ are chosen such that they coincide with the doubly symmetric axes of the cross-section where $X$-axis is along the diameter. The ring is supported at both ends of a diameter. At one end, that is, the origin of coordinates $(X, Y, Z)$, the ring is completely fixed. At the other end, it is free to move and to rotate only along and around the $X$-axis. At this end, an external moment is applied about $X$-axis.

Considering the symmetry of the structure along with the antisymmetry of the applied moment, the structural model shown in Fig. 3 can be simplified and we have only to analyze either 1/2 or 1/4 of the original model, as illustrated in Fig. 4. It should be noted for the 1/4 model that the rotational angle about the $X$-axis is equivalent to a half of the corresponding value for the original model. To discretize the structural system, the 1/4 model requires fewer finite elements. However, as a result of our numerical analysis, the convergence of the 1/2 model in the Newton Raphson iterative procedures turned out to be faster than that of the 1/4 model. Further, the number of finite elements is not so crucial in our transfer matrix method as in the conventional stiffness method. Thus, we here adopt the 1/2 model in our numerical analysis. With this model, the analysis of the deployable rings is reduced to the solution of a two-point boundary value problem.

In view of the simplicity of analysis, the above ring model is approximated by the assemblage of straight elements.

## 3. ANALYSIS OF RODS ACCOMPANYING FINITE ROTATIONS IN THREE-DIMENSIONAL SPACE

The buckling behavior of our concern accompanies very large rotations in three-dimensional space. Thus, we have to use an accurate method of analysis which precisely takes into account the geometrical non-linearity of the rod behavior. Since we have already developed a numerical method (Goto *et al.*, 1988) which satisfies this requirement, a brief explanation is made about this method.

### (a) *Governing differential equations of rods under small strains*

Here, we describe the governing differential equations of the rod model on which our numerical method is based. Considering that the material of the deployable rings must remain elastic during the buckling process, it is expected that the strains remain negligibly small compared with unity even in the case when the ring undergoes extremely large rotations. Thus, the governing differential equations adopted here are those of the theory of *finite displacements and small strains*. These equations are derived from the exact governing equations of *finite displacements and finite strains* (Goto *et al.*, 1985), simplified by introducing the assumption of small strains. As can be seen from this assumption, these governing equations have no restrictions on the magnitude of the finite rotations, as long as the strains are small. In addition to the assumption of small strain, we introduce the customary beam assumptions of no deformation within the cross-section and no shear of the cross-section with respect to the beam axis.

In order to express the governing differential equations, we consider an originally straight element shown in Fig. 5, and introduce a local Cartesian coordinate system $(x, y, z)$

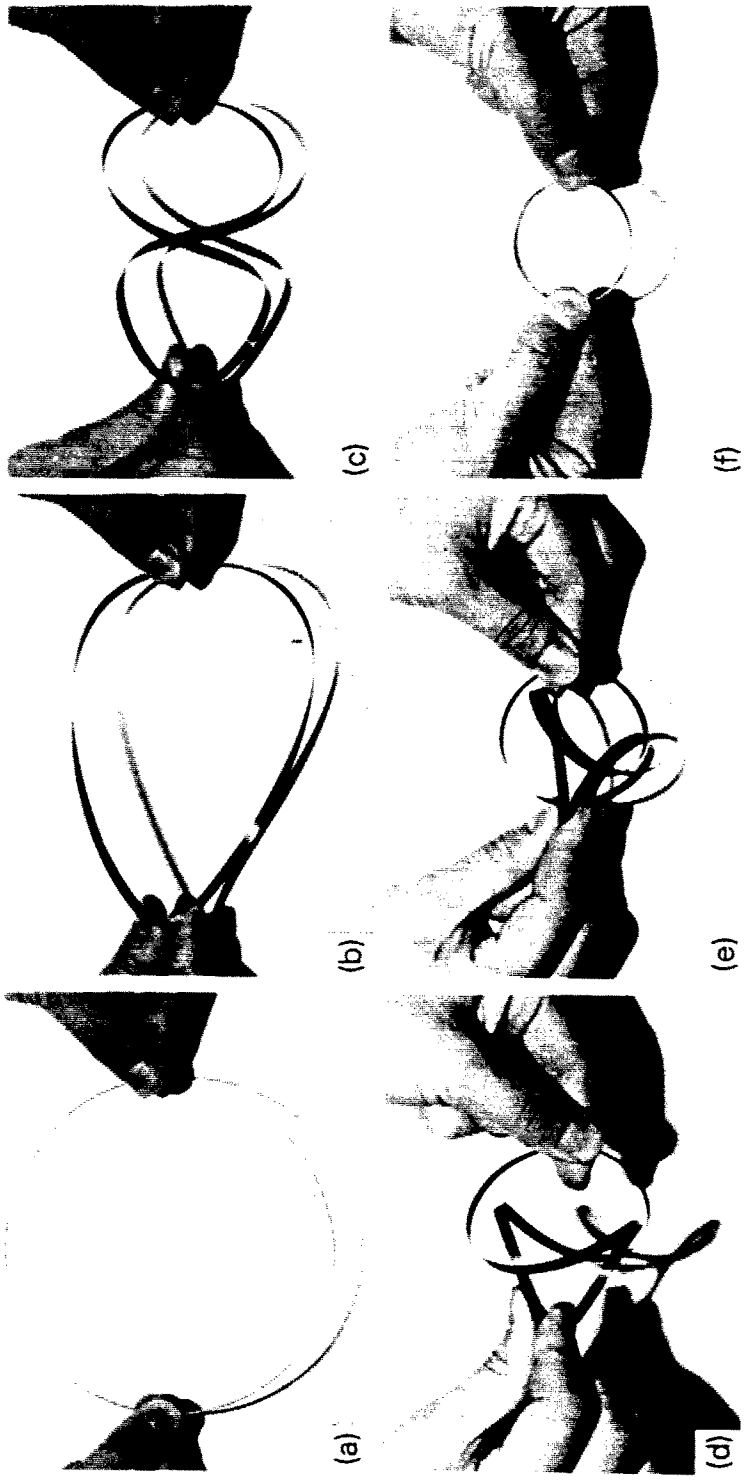


Fig. 2. Experimental transformation process of a deployable ring.

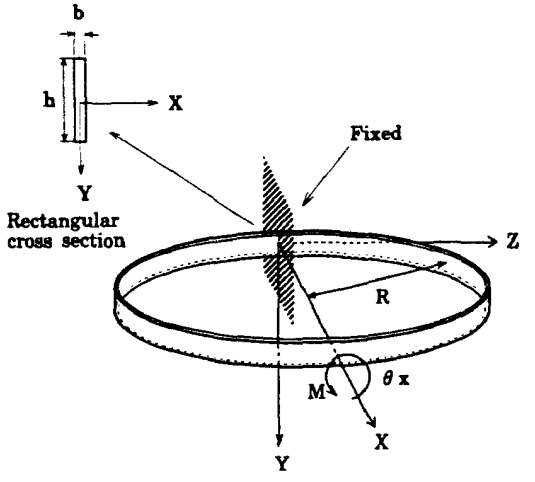


Fig. 3. Ring model and global coordinates.

with base vectors $(\mathbf{g}_x, \mathbf{g}_y, \mathbf{g}_z)$. Based on this coordinate system, the four deformation components $(\kappa_x, \kappa_y, \tau, \varepsilon_0)$, representing the deformation of the centroidal axis of the element, are defined as follows:

$$\frac{\mathrm{d}}{\mathrm{d}z}\begin{Bmatrix}\hat{\mathbf{i}}_{x0}\\ \hat{\mathbf{i}}_{y0}\\ \hat{\mathbf{i}}_{z0}\end{Bmatrix} = [D]\begin{Bmatrix}\hat{\mathbf{i}}_{x0}\\ \hat{\mathbf{i}}_{y0}\\ \hat{\mathbf{i}}_{z0}\end{Bmatrix}, \quad \hat{\mathbf{g}}_{x0} = (1+\varepsilon_0)\hat{\mathbf{i}}_{z0}, \quad [D] = \begin{bmatrix} 0, & \tau, & -\kappa_y \\ -\tau, & 0, & -\kappa_x \\ \kappa_y, & -\kappa_x, & 0 \end{bmatrix}, \qquad \text{(1a–c)}$$

where $(\hat{\mathbf{i}}_{x0}, \hat{\mathbf{i}}_{y0}, \hat{\mathbf{i}}_{z0})$ are the unit vectors obtained by normalizing the deformed base vectors

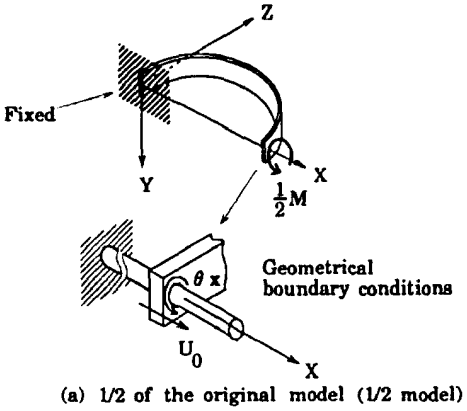


(a) 1/2 of the original model (1/2 model)

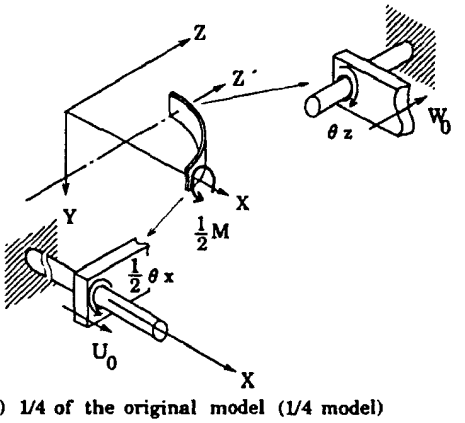


(b) 1/4 of the original model (1/4 model)

Fig. 4. Simplification of the original model.

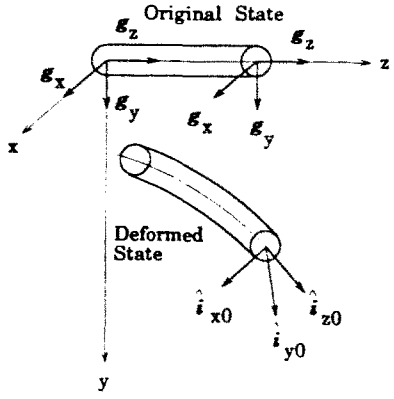


Fig. 5. Coordinate system for a straight element.

$(\hat{\mathbf{g}}_{x0}, \hat{\mathbf{g}}_{y0}, \hat{\mathbf{g}}_{z0})$ on the centroidal axis which are orthogonal due to beam assumptions. Physically, $(\kappa_x/(1+\varepsilon_0), \kappa_y/(1+\varepsilon_0), \tau/(1+\varepsilon_0)$, and $\varepsilon_0$ correspond to the components of curvature about the deformed base vectors $(\hat{\mathbf{g}}_{x0}, \hat{\mathbf{g}}_{y0})$, the torsional rate and the extensional rate, respectively, of the deformed controidal axis.

With the deformation components defined above, the equilibrium equations are derived through the principle of virtual work by introducing beam assumptions together with the condition of small strains.

The constitutive relations are assumed to follow the linear elastic relations as

$$\sigma_{zz} = Ee_{zz}, \quad \sigma_{zx} = 2Ge_{zx}, \quad \sigma_{zy} = 2Ge_{zy} \tag{2a-c}$$

in which stress and strain are second Piola-Kirchhoff stress tensor and Green strain tensor, respectively, defined in terms of the $(x, y, z)$ coordinates. Under the condition of small strains along with the beam assumptions, eqns (2a-c) are reduced to

$$\sigma_{zz} = E(\varepsilon_0 + y\kappa_x - x\kappa_y), \quad \sigma_{zx} = -Gy\tau, \quad \sigma_{zy} = Gx\tau. \tag{3a-c}$$

The present constitutive relations coincide with those defined between physical components of stress and strain (Fung, 1965), as long as the small strain condition holds.

The governing differential equations derived from the above procedures are summarized in Table 1. These governing equations for rods are similar to Kirchhoff's equations (Love, 1944) except that our equations consider the effect of elongation of the centroidal axis.

Although the governing differential equations in Table 1 are expressed by the deformation components defined by eqns (1a-c), these deformation components can be related to the translational and the rotational displacement components. If we express the translational displacements by the components $(u_0, v_0, w_0)$ in the directions of the base vectors $(\mathbf{g}_x, \mathbf{g}_y, \mathbf{g}_z)$ and the rotational displacements by the directional cosines $[l_{ih}]$ of vectors $(\hat{\mathbf{i}}_{x0}, \hat{\mathbf{i}}_{y0}, \hat{\mathbf{i}}_{z0})$ referred to the base vectors $(\mathbf{g}_x, \mathbf{g}_y, \mathbf{g}_z)$ as

$$\begin{Bmatrix} \hat{\mathbf{i}}_{x0} \\ \hat{\mathbf{i}}_{y0} \\ \hat{\mathbf{i}}_{z0} \end{Bmatrix} = [l_{ih}] \begin{Bmatrix} \mathbf{g}_x \\ \mathbf{g}_y \\ \mathbf{g}_z \end{Bmatrix}, \quad [l_{ih}] = \begin{bmatrix} l_{xx}, & l_{xy}, & l_{xz} \\ l_{yx}, & l_{yy}, & l_{yz} \\ l_{zx}, & l_{zy}, & l_{zz} \end{bmatrix}, \tag{4a,b}$$

the deformation components and the displacement components are related to each other as shown below:

$$\mathrm{d}[l_{ih}]/\mathrm{d}z = [D][l_{ih}], \quad u_0' = (1+\varepsilon_0)l_{zx}, \quad v_0' = (1+\varepsilon_0)l_{zy}, \quad w_0' = (1+\varepsilon_0)l_{zz} - 1, \tag{5a-d}$$

Table 1. Governing equations for space rods

| Equilibrium equations | Constitutive equations |
|---|---|
| $F_x' - F_y\tau + F_z\kappa_y = 0$ | $N = EA\varepsilon_0$ |
| $F_y' + F_x\tau - F_z\kappa_x = 0$ | $M_x = -EI_{xx}\kappa_y, \quad M_y = EI_{yy}\kappa_x, \quad M_z = GJ\tau$ |
| $F_z' + F_y\kappa_x - F_x\kappa_y = 0$ | where |
| $M_z' - M_y\kappa_y - M_z\kappa_x = 0$ | $M_x = \int_A \sigma_{zz} x \, dA, \quad M_y = \int_A \sigma_{zz} y \, dA$ |
| where | |
| $F_x = M_x' - M_y\tau + M_z\kappa_x$ | $M_z = \int_A (\sigma_{zy} x - \sigma_{zx} y) \, dA$ |
| $F_y = M_y' + M_x\tau + M_z\kappa_y$ | |
| $F_z = N$ | $A = \int_A dA, \quad I_{xx} = \int_A x^2 \, dA, \quad I_{yy} = \int_A y^2 \, dA$ |
| | $J = \begin{cases} \cdot \text{Circular cross-section (radius } = r) \\ \quad = \int_A (x^2 + y^2) \, dA = \pi r^4/2 \\ \cdot \text{Rectangular cross-section } (b \times h) \\ \quad \text{(Timoshenko } et\ al., \text{ 1970)} \\ \quad = \frac{b^3 h}{3}\left\{1 - \frac{192b}{\pi^5 h}\sum_{n=1}^{\infty}\frac{1}{(2n-1)^5}\tanh\frac{(2n-1)\pi h}{2b}\right\} \end{cases}$ |

Remarks: $(\cdot)' = d(\cdot)/dz$, $\int_A dA$ = Integration over the cross-sectional area.

where $'$ denotes the differentiation with respect to $z$. It should be noted for the directional cosines $[l_{ab}]$ that three components out of nine are independent.

(b) *Numerical analysis based on the transfer matrix technique*

We shall explain a numerical method (Goto *et al.*, 1988) to solve the aforementioned non-linear governing differential equations of space rods. In this method, the transfer matrix technique was expanded into non-linear range.

In the first place, we derive the *field transfer equations* which transfer the nodal physical quantities from node $i$ to $i+1$ of a finite element.

The state vector $\{Q_j\}$ which consists of these physical quantities is defined by

$$\{Q_j\} = (u_0, v_0, w_0, \quad [l_{ab}], \quad \bar{F}_x, \bar{F}_y, \bar{F}_z, \quad \bar{M}_y, -\bar{M}_x, \bar{M}_z), \tag{6}$$

in which $(\bar{F}_x, \bar{F}_y, \bar{F}_z)$ and $(\bar{M}_y, -\bar{M}_x, \bar{M}_z)$ are components of sectional force $\mathbf{F}$ and sectional moment $\mathbf{M}$, respectively defined as

$$\mathbf{F} = \bar{F}_x\mathbf{g}_x + \bar{F}_y\mathbf{g}_y + \bar{F}_z\mathbf{g}_z, \quad \mathbf{M} = \bar{M}_y\mathbf{g}_x - \bar{M}_x\mathbf{g}_y + \bar{M}_z\mathbf{g}_z. \tag{7a-b}$$

As can be seen from eqn (6), the directional cosines $[l_{ab}]$ are adopted herein to express the rotational displacements. Although $[l_{ab}]$ contains nine components, only three components are independent.

Using the Taylor expansion at node $i$, the components of the state vector at node $i+1$ are given by

$$Q_j|_{i+1} = Q_j|_i + \sum_{n=1}^{\infty} Q_j^{(n)}|_i (\Delta z)^n/n! \quad (1 \leqslant j, k \leqslant 18), \tag{8}$$

where $Q_j^{(n)}|_i$ denotes the $n$th order derivative of $Q_j$ at node $i$ and $\Delta z$ is the element length. in order for eqn (8) to be used as the field transfer equations, $Q_j^{(n)}|_i$ has to be expressed explicitly by the components of the state vector $\{Q_j|_i\}$ at node $i$. For this purpose, the governing equations in Table 1, together with eqn (5) are transformed into the first order

differential equations in terms of the components of the state vector, as summarized in Table 2. Then, the derivative $Q_j^{(n)}|_i$ can be obtained by successive differentiation and substitution of these first order differential equations. As shown in the Appendix, $Q_j^{(n)}|_i$ is derived up to the second derivative and the higher order terms are truncated in eqn (8). Finally, the field transfer equations can be expressed in the form

$$Q_j|_{i+1} = T_j(Q_1|_i, \ldots, Q_{18}|_i) \quad (1 \leqslant j \leqslant 18). \tag{9}$$

The field transfer equations are non-linear in terms of the components of the state vector. So the basic algebraic equations involved in the present problem also become non-linear and some iterative procedure is required to solve them. As an iterative procedure, we here employ the incremental arc-length method combined with the *Newton–Raphson iterative procedures*. For this purpose, we have to derive from eqn (9) the incremental field transfer equations linearized in terms of the components of the incremental state vector. In these incremental equations, the small incremental directional cosines $[\Delta l_{ab}]$ are replaced by the incremental rotational angles $(\Delta\alpha_x, \Delta\alpha_y, \Delta\alpha_z)$ about the base vectors $(\mathbf{g}_x, \mathbf{g}_y, \mathbf{g}_z)$. This replacement is based on the relation given by

$$[\Delta l_{ab}] = [l_{ab}]\begin{bmatrix} 0, & \Delta\alpha_z, & -\Delta\alpha_y \\ -\Delta\alpha_z, & 0, & \Delta\alpha_x \\ \Delta\alpha_y, & -\Delta\alpha_x, & 0 \end{bmatrix}. \tag{10}$$

The use of the above incremental rotational angles as components of the state vector makes it possible to express the incremental field transfer equations in the matrix form

$$\{\Delta Q_j^*|_{i+1}\} = [\Delta T_{j,k}]\{\Delta Q_k^*|_i\} \quad (1 \leqslant j,k \leqslant 12), \tag{11}$$

where $[\Delta T_{j,k}]$ is the incremental field transfer matrix and $\{\Delta Q_j^*\}$ is expressed as

$$'\{\Delta Q_j^*\} = \{\Delta u_0, \Delta v_0, \Delta w_0, \Delta\alpha_x, \Delta\alpha_y, \Delta\alpha_z, \Delta\bar{F}_x, \Delta\bar{F}_y, \Delta\bar{F}_z, \Delta\bar{M}_y, -\Delta\bar{M}_x, \Delta\bar{M}_z\}. \tag{12}$$

This form is exactly the same as that of the field transfer equations for the small displacement

Table 2. First order differential equations

$$u_0' = \{1 + (l_{1x}\bar{F}_x + l_{2x}\bar{F}_y + l_{3x}\bar{F}_z)/EA\}l_{3x}$$
$$v_0' = \{1 + (l_{1x}\bar{F}_x + l_{2y}\bar{F}_y + l_{3z}\bar{F}_z)/EA\}l_{3y}$$
$$w_0' = \{1 + (l_{1z}\bar{F}_x + l_{2y}\bar{F}_y + l_{3z}\bar{F}_z)/EA\}l_{3z} - 1$$

$$[l_{ab}]' = \begin{bmatrix} 0, & M_z/GJ, & M_x/EI_x \\ -M_z/GJ, & 0, & M_y/EI_y \\ -M_x/EI_x, & -M_y/EI_y, & 0 \end{bmatrix}[l_{ab}]$$

$$\bar{F}_x' = 0$$
$$\bar{F}_y' = 0$$
$$\bar{F}_z' = 0$$

$$\bar{M}_x' = (l_{1x}l_{3y} - l_{1y}l_{3x})\bar{F}_x + (l_{2y}l_{3x} - l_{3y}l_{2x})\bar{F}_z$$
$$\bar{M}_y' = (l_{1x}l_{3y} - l_{1y}l_{3x})\bar{F}_y + (l_{1x}l_{3z} - l_{3x}l_{1z})\bar{F}_z$$
$$\bar{M}_z' = (l_{3x}l_{2y} - l_{3y}l_{2x})\bar{F}_z + (l_{1z}l_{3y} - l_{3z}l_{1y})\bar{F}_y$$

where

$$\begin{Bmatrix} M_x \\ -M_y \\ M_z \end{Bmatrix} = [l_{ab}]\begin{Bmatrix} \bar{M}_x \\ -\bar{M}_y \\ \bar{M}_z \end{Bmatrix}$$

theory. Further, the small rotational angles $(\Delta\alpha_x, \Delta\alpha_y, \Delta\alpha_z)$ can be treated as components of a vector quantity. Thus, the usual techniques of the transfer matrix method (Kersten, 1962; Pestel and Leckie, 1963; Livesley, 1964) can be applied to the incremental equations.

In the present ring model approximated by the assemblage of straight elements, the centroidal axes of adjacent elements are not parallel to each other, as illustrated in Fig. 6. Thus, in addition to the field transfer equations, we have to derive the *point transfer equations* which transfer the state vector from the left to the right at a node. These point transfer equations are also necessary, if concentrated loads are applied at a node.

Suppose elements $i$ and $i+1$ are rigidly connected to each other at node $i+1$, as in Fig. 6. The directional cosines $[L_{ab}]_{i+1}$ of the element coordinates $(x^{i+1}, y^{i+1}, z^{i+1})$ are defined in terms of the adjacent element coordinates $(x^i, y^i, z^i)$ as

$$\begin{Bmatrix} \mathbf{g}_x \\ \mathbf{g}_y \\ \mathbf{g}_z \end{Bmatrix}^{i+1} = [L_{ab}]_{i+1} \begin{Bmatrix} \mathbf{g}_x \\ \mathbf{g}_y \\ \mathbf{g}_z \end{Bmatrix}^{i}. \tag{13}$$

$\mathbf{F}^c_{i+1}$ and $\mathbf{M}^c_{i+1}$ in Fig. 6 are the concentrated force and moment, respectively applied at node $i+1$, and the $(x^{i+1}, y^{i+1}, z^{i+1})$-components of these concentrated loads are defined by

$$\mathbf{F}^c_{i+1} = F^c_{x^{i+1}}\mathbf{g}_{x^{i+1}} + F^c_{y^{i+1}}\mathbf{g}_{y^{i+1}} + F^c_{z^{i+1}}\mathbf{g}_{z^{i+1}},$$
$$\mathbf{M}^c_{i+1} = M^c_{x^{i+1}}\mathbf{g}_{x^{i+1}} + M^c_{y^{i+1}}\mathbf{g}_{y^{i+1}} + M^c_{z^{i+1}}\mathbf{g}_{z^{i+1}}. \tag{14a,b}$$

Considering equilibrium and compatibility, the point transfer equations at node $i+1$ can be given for the components of the state vector as

$$\begin{Bmatrix} u_{0^{i+1}} \\ v_{0^{i+1}} \\ w_{0^{i+1}} \end{Bmatrix}^{i+1} = [L_{ab}]_{i+1} \begin{Bmatrix} u_{0^{i+1}} \\ v_{0^{i+1}} \\ w_{0^{i+1}} \end{Bmatrix}^{i},$$

$$[l_{\dot{a}b}|_{i+1}]^{i+1} = [L_{ab}]_{i+1}[l_{\dot{a}b}|_{i+1}]^{i}[L_{ab}]_{i+1},$$

$$\begin{Bmatrix} F_{x^{i+1}} \\ F_{y^{i+1}} \\ F_{z^{i+1}} \end{Bmatrix}^{i+1} = [L_{ab}]_{i+1} \begin{Bmatrix} F_{x^{i+1}} \\ F_{y^{i+1}} \\ F_{z^{i+1}} \end{Bmatrix}^{i} + \begin{Bmatrix} \bar{F}^c_{x^{i+1}} \\ \bar{F}^c_{y^{i+1}} \\ \bar{F}^c_{z^{i+1}} \end{Bmatrix},$$

$$\begin{Bmatrix} M_{y^{i+1}} \\ -M_{x^{i+1}} \\ M_{z^{i+1}} \end{Bmatrix}^{i+1} = [L_{ab}]_{i+1} \begin{Bmatrix} M_{y^{i+1}} \\ -M_{x^{i+1}} \\ M_{z^{i+1}} \end{Bmatrix}^{i} + \begin{Bmatrix} \bar{M}^c_{x^{i+1}} \\ \bar{M}^c_{y^{i+1}} \\ \bar{M}^c_{z^{i+1}} \end{Bmatrix}. \tag{15a-d}$$

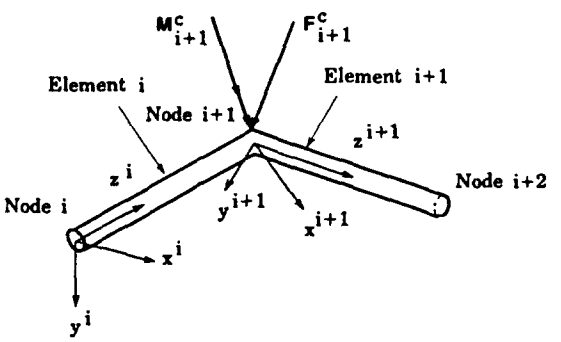


Fig. 6. Nodes of elements in the original state.

The incremental point transfer equations are derived as follows, by taking the increment of eqns (15) and introducing the incremental rotational angles from eqn (10)

$$\{\Delta Q_j^*|_{i+1}\}^{i+1} = [\Delta P_{j,k}]^{i+1}\{\Delta Q_k^*|_{i-1}\}^i + \{\Delta Q_j^{*c}|_{i+1}\}^{i+1}, \tag{16}$$

where $[\Delta P_{j,k}]^{i+1}$ is the incremental point transfer matrix at node $i+1$ and $\{\Delta Q_j^{*c}|_{i+1}\}^{i+1}$ is given by

$$\{\Delta Q_j^{*c}|_{i+1}\}^{i+1} = \{0,0,0,0,0,0,\Delta\bar{F}_{x^*}^c{}_{i+1},\Delta\bar{F}_{y^*}^c{}_{i+1},\Delta\bar{F}_{z^*}^c{}_{i+1},\Delta\bar{M}_{x^*}^c{}_{i+1},\Delta\bar{M}_{y^*}^c{}_{i+1},\Delta\bar{M}_{z^*}^c{}_{i+1}\}. \tag{17}$$

In the incremental arc-length method, eqns (11) and (16) as well as an equation to control the increment of the arc-length of equilibrium paths (Riks, 1979) are used to calculate the increments of the state vector at node 1. Since these equations are linearized, the increment of the state vector at node 1 so obtained is approximate and the Newton–Raphson method is employed to correct the approximate values. The corrections are made, based on the errors of the state vector at the end node, i.e. node $n$. These errors are known by comparing the prescribed boundary values with those of the state vector obtained by transferring the approximate state vector from node 1 to node $n$, using eqns (9) and (15) (Goto *et al.*, 1988).

## 4. BUCKLING BEHAVIOR OF RINGS

(a) *Governing structural parameters*

In order to examine the general buckling behavior of deployable rings, we first clarify the governing structural parameters. These parameters can be found out as follows, by first considering the geometrical parameters of rings and then non-dimensionalizing the field transfer equations of eqn (9),

$$I_{xx}/J, \quad I_{yy}/J, \quad J/(AR^2), \quad E/G, \quad A/R^2. \tag{18a–e}$$

For simplicity, we here restrict our attention to steel rings. Then, the value of $E/G$ becomes constant, i.e. $E/G \approx 2.6$. Further, if the rings are supposed to have a rectangular cross-section ($h \times b$) as shown in Fig. 3, independent structural parameters decrease. That is, noting from Table 1 that the constants for a rectangular cross-section are given by

$$A = bh, \quad I_{XX} = b^3h/12, \quad I_{YY} = bh^3/12,$$
$$J = \frac{b^3h}{3}\left\{1 - \frac{192b}{\pi^5 h}\sum_{n=1}^{\infty}\frac{1}{(2n-1)^5}\tanh\frac{(2n-1)\pi h}{2b}\right\}, \tag{19a–d}$$

the independent parameters are finally reduced to

$$h/b, \quad R/h. \tag{20a,b}$$

(b) *Application of numerical analysis*

We shall discuss the application of the numerical method to the buckling analysis of the deployable rings. As an example, we choose a ring with a rectangular cross-section whose structural parameters are $h/b = 3$ and $R/h = 20$.

Our analysis is based on the approximate field transfer equations derived by truncating the higher order terms with respect to the element length. Further, the shape of the ring is approximated by the assemblage of straight elements. Thus, it is important to know the necessary number of finite elements which yield convergent solutions. As an important

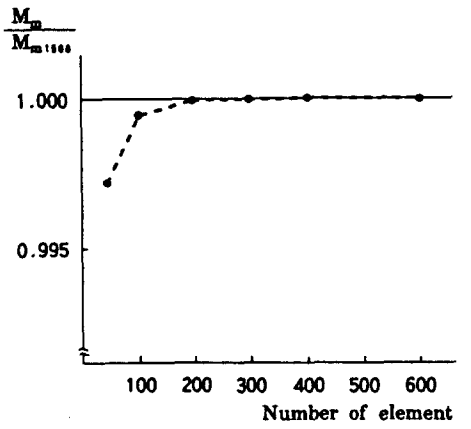


Fig. 7. Convergence of the maximum moment $M_m$ applied in buckling process.

physical quantity most sensitive to this discretization, we show in Fig. 7 the convergence of the maximum moment $M_m$ applied in the buckling process. In this figure the moment is normalized by the maximum moment $M_{m_{1500}}$ for the model where half of the ring is divided into 1500 equal finite elements. In view of the convergence in Fig. 7, 200 elements are enough for the 1/2 model.

With the ring model discretized above, we analyze the buckling behavior of the deployable ring unit it is transformed to a small ring. Representing the calculated results, we show in Fig. 8 the relation between the non-dimensionalized external moment $MR/EI_{YY}$ and the rotational angle $\theta_X$ about the $X$-axis at the location where the external moment is applied by the arc-length control. Further, at every $\pi/4$ radians in terms of the rotational angle $\theta_X$, the deformed configurations of the ring are illustrated in Fig. 9. These deformed configurations correspond to the points marked by (1)–(9) on the equilibrium path in Fig. 8. As can be seen from this figure, our numerical analysis accurately simulates the following characteristics of the buckling behavior of the deployable ring. First, the ring deforms accompanying considerably large rotations in three-dimensional space and is finally transformed to a small ring with a diameter of one-third of its original size. Second, the final shape is in the equilibrium state without any external moment.

(c) *Effect of structural parameters on buckling behavior*

Using the numerical analysis explained above, we herein investigate the effect of the structural parameters on the buckling behavior of the rings with rectangular cross-sections.

First we examine how the $MR/EI_{YY}-\theta_X$ relation shown in Fig. 8 is affected by the structural parameters: $h/b$ and $R/h$. The results are summarized in Fig. 10. In this figure, the result for a ring with a circular cross-section is also included for comparison. As seen from eqns (18a–e) together with the definitions of the circular cross-sectional constants in

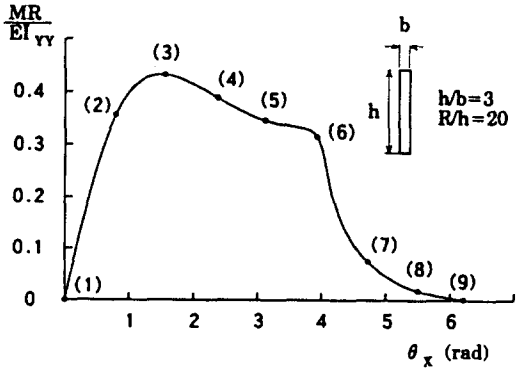


Fig. 8. Moment–rotation curve of the ring with $h/b = 3$ and $R/h = 20$.

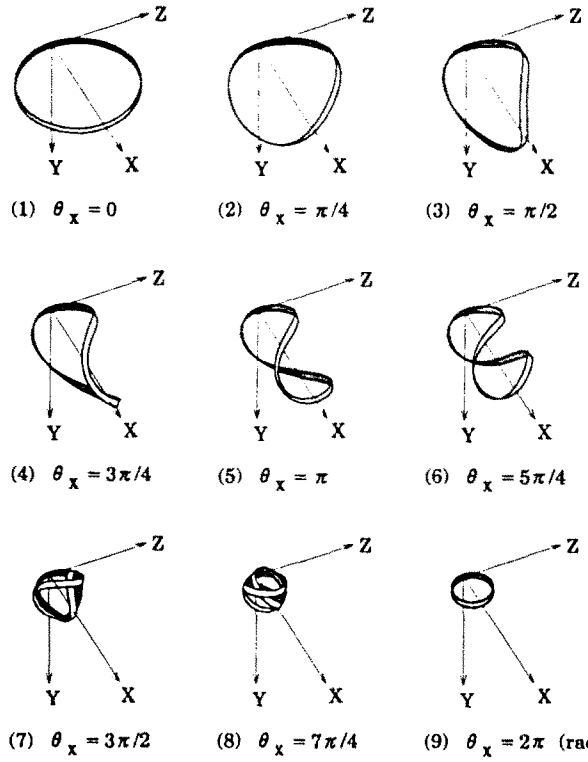


Fig. 9. Theoretical transformation process of the deployable ring with $h/b = 3$ and $R/h = 20$.

Table 1, the buckling behavior for this case is governed only by the structural parameter of $R/r$ where $r$ is the radius of the cross-section.

From Fig. 10, it can be seen that the buckling behavior is very much influenced by the parameter $h/b$. That is, for a ring with a smaller value of $h/b$, a larger moment is required to buckle it. Further, in case when $h/b \leqslant 1.51$ or the ring has a circular cross-section, the ring cannot be transformed to a small ring. For the rings with rectangular cross-sections, the boundary value $\mu^*$ of the parameter $h/b$ below which this transformation becomes

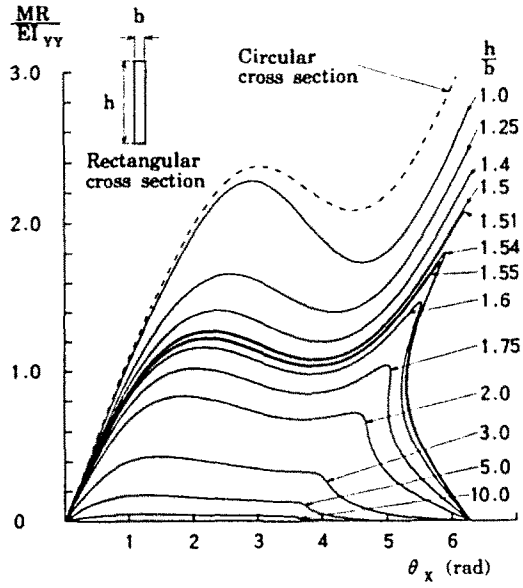


Fig. 10. Moment–rotation curves of rings with various kinds of cross-sectional parameters.

impossible is known to exist somewhere in the range $1.51 \leqslant \mu^* < 1.54$. However, a more detailed boundary cannot be identified, because the present numerical analysis becomes unstable in this range. Since the shapes of the equilibrium curves in Fig. 10 change drastically from one side of the boundary to the other, the equilibrium curve for the boundary value $h/b = \mu^*$ is expected to have a bifurcation point, as is schematically shown in Fig. 11. Thus, for the rings with $h/b$ very close to the boundary value $\mu^*$ and in the range of $h/b > \mu^*$, their equilibrium curves will have a limit point with very high curvature which numerically results in a singular tangent system matrix. This is considered to be the chief reason for the numerical instability.

As for the other structural parameter $R/h$ or $R/r$, we cannot determine its effect on the $MR/EI_{YY}-\theta_X$ relationship, as far as we examine the realistic range of $5 \leqslant (R/h, R/r) \leqslant 50$. Thus, the value of $R/h$ or $R/r$ is not noted in Fig. 10. As the governing differential equations of the deployable rings become highly non-linear, we cannot theoretically verify the above numerical results. However, if we restrict the problem to the small displacement range, the following relation holds:

$$\theta_X = \frac{\pi}{2}\left(1 + \frac{EI_{YY}}{GJ} + \frac{8EI_{YY}}{\pi^2 GJ}\right)\frac{MR}{EI_{YY}}. \tag{21}$$

Noting that eqn (21) does not include the parameter $R/h$ or $R/r$, we can partly confirm that the numerical results are not affected by this parameter.

It is known from the aforementioned considerations on the buckling behavior that the rectangular cross-sectional shapes of the deployable rings must satisfy the requirement that $h/b \geqslant \mu^*$ in order for the rings to be transformed to small rings. In addition to the above requirement, the maximum stress $\sigma_{max}$ produced in the buckling process must not exceed the elastic limit of the ring material. In view of this requirement, we shall next investigate the influence of the structural parameters on this maximum stress $\sigma_{max}$. As a realistic range, we examine the rings with the parameters $5 \leqslant h/b \leqslant 50$ and $5 \leqslant R/h \leqslant 50$. Representing the calculated results, we demonstrate in Figs 12 and 13 the change of the axial stress at the fixed end which is most significant in the model illustrated in Fig. 4(a). Most of this axial stress is due to the bending moment about the minor axis of the cross-section. It should be noted that the axial stress with the same magnitude is also produced at the other end of this model because of its symmetry. As seen from Figs 12 and 13, the maximum stress increases with the decrease of the parameters $R/h$ and $h/b$. Since this maximum stress almost coincides with the stress in the final configuration, the maximum stress is approximated well by

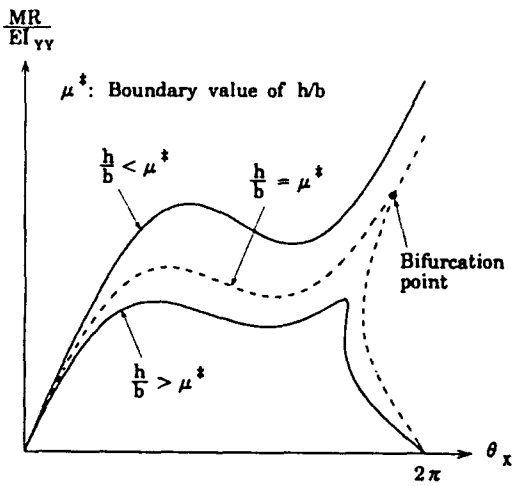


Fig. 11. Expected behavior of a ring for the boundary value of $h/b$.

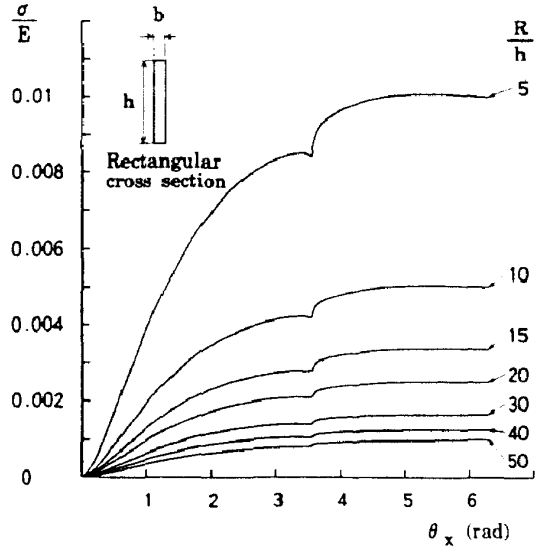


Fig. 12. Axial stress at the fixed end of rings with $h/b = 20$.

$$\frac{\sigma_{max}}{E} \approx \frac{1}{(R/h)(h/b)}. \tag{22}$$

Besides the axial stress, a shear stress is produced in the ring. However, this value is less than 1/100 of the axial stress and is negligibly small. Thus, the requirement for the rings to be elastic is approximately expressed from eqn (22) in terms of the structural parameters as

$$(R/h)(h/b) \gtrsim E/\sigma_y, \tag{23}$$

where $\sigma_y$ is the tensile or the compressive yield stress.

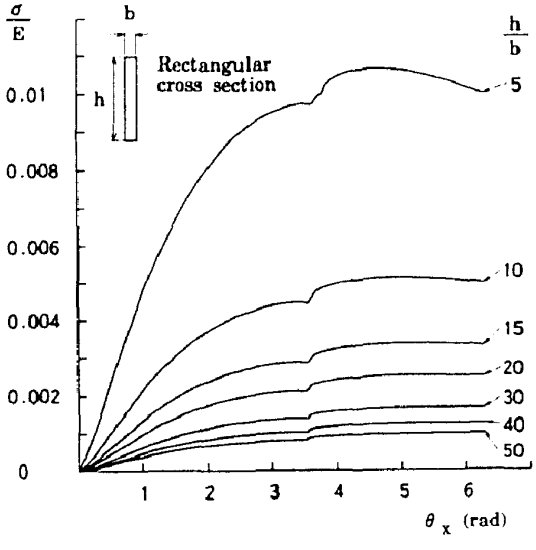


Fig. 13. Axial stress at the fixed end of rings with $R/h = 20$.

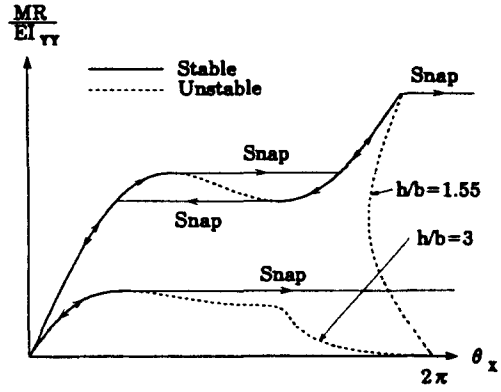


Fig. 14. Stability and response of deployable rings under load control.

## 5. TRANSFORMATION PROCEDURES OF DEPLOYABLE RINGS

In the previous section, the requirements of the deployable rings are examined in terms of the structural parameters. We here discuss the control method which should be adopted in their transformation process. Theoretically, it is possible to use the versatile arc-length control as we did in the present numerical analysis. In reality, we, however, have to use either the load- or the displacement-control method due to the limitations of loading devices. Therefore, we examine the applicability of these two control methods.

In Fig. 14, the stability of the equilibrium curves under the load control are illustrated for two specific cases with or without a *snap-back* behavior. In our analysis, the stability of the rings on the equilibrium curves can be identifed by the minimum eigenvalue of the tangent stiffness matrix except the critical points. That is, the structural system is stable or unstable according to whether the minimum eigenvalue is positive or negative. From Fig. 14, it can be seen that the unloading equilibrium path starting from the maximum point of moment is unstable. So, the system will snap dynamically after the maximum moment is reached. This indicates that the transformation to a small ring is impossible under the load control.

In the same manner as in Fig. 14, we show in Fig. 15 the stability of the equilibrium paths when the structural systems are controlled by the rotational angle $\theta_x$. In view of reality, the loading device is assumed here to have the finite torsional rigidity of $K_M$ which is greater than the absolute value of the tangent stiffness of the equilibrium curve at $\theta_x = 2\pi$. This assumption ensures the stability of the transformed shape of the rings. With the above loading device, we have the inclined loading lines with the gradient of $-K_M R/EI_{YY}$ in the $MR/EI_{YY}-\theta_X$ diagram and the snaps occur where these lines touch the equilibrium curve (Thompson and Hunt, 1984). From Fig. 15, it can be seen that the transformation into a small ring is possible under the displacement control.

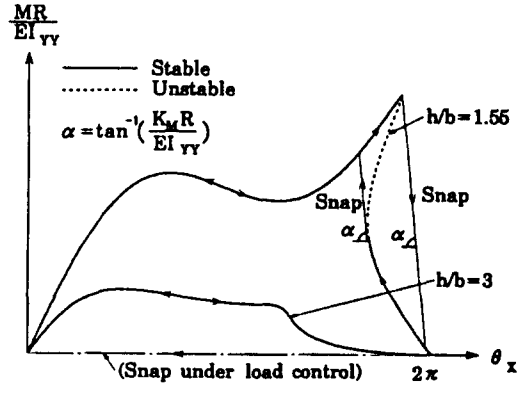


Fig. 15. Stability and response of deployable rings under displacement control by a loading device with the torsional rigidity of $K_M$.

Regarding the deployment, the ring will return to its original configuration either by the load control or the displacement control, as shown in Fig. 15. In the case of the load control, the transformed equilibrium state is unstable. So, the ring snaps dynamically back to the original configuration, if we remove the restraint. This implies that the rings have a self-contained ability for deployment.

## 6. CONCLUDING REMARKS

We have theoretically examined an interesting buckling phenomenon of a ring which could be applied to a deployable ring. Since this buckling behavior accompanies extremely large rotations in three dimensional space, we have used a method of analysis which precisely takes into account the geometrical non-linearity of space rods. As a result of this buckling analysis, it has been demonstrated that the ring is transformed to a small ring with a diameter of one-third of its original size. Further, the transformed shape is maintained without any external forces. This buckling phenomenon, however, does not always occur for rings with arbitrary cross-sectional shapes. That is, although the buckling phenomenon has been confirmed for the rings with the rectangular cross-sections ($h \times b$) of $h/b \geqslant 1.54$, this phenomenon does not occur for the rings with the rectangular cross-sections of $h/b \leqslant 1.51$ or those with circular cross-sections. In order for a ring to be deployable, the maximum stress produced during the buckling process is also required to remain within the elastic range. This requirement is approximately given by $(R/h)(h/b) \geq E/\sigma_y$, where $E$ is Young's modulus, $R$ is the radius of a ring and $\sigma_y$ is the tensile or the compressive yield stress. Regarding the transformation procedure, the ring can be transformed to a small ring only by the displacement model. In this case, the torsional rigidity of the loading devices has to be greater than the absolute value of the tangent stiffness of the equilibrium curves at $\theta_z = 2\pi$. The deployment of the transformed small rings is, however, possible either by the load control or the displacement control. In the case of the load control, the ring snaps dynamically back to the original configuration if we remove the restraint. This implies that the ring is self-contained in terms of deployment.

*Acknowledgement*—The authors are grateful for the reviewers' valuable comments in preparing the revised version of this paper.

## REFERENCES

Antman, S. S. (1972). The theory of rods. *Handbuch der Physik*. Vol. VIa/2. Springer, Berlin.
Antman, S. S. (1974). Kirchhoff problem for nonlinearly elastic rods. *Q. Appl. Math.* **32**(3), 221–240.
Bathe, K. J. and Bolourchi, S. (1979). Large displacement analysis of space frames. *Int. J. Num. Methods Engng* **14**, 961–986.
Fung, Y. C. (1965). *Foundations of Solids Mechanics*. Prentice-Hall, New Jersey.
Goto, Y., Matsuura, S., Hasegawa, A. and Nishino, F. (1985). A new formulation of finite displacement theory of curved and twisted rods. *Struct. Engng/Earthquake Engng*, JSCE **2**(2), 365s–375s.
Goto, Y., Morikawa, Y. and Matsuura, S. (1988). Direct Lagrangian non-linear analysis of elastic space rods using transfer matrix technique. *Struct. Engng/Earthquake Engng*, JSCE **5**(a), 151s–160s.
Kersten, R. (1962). *Das Reduktionsverfahren der Baustatik*. Springer, Berlin.
Livesley, R. K. (1964). *Matrix Methods of Structural Analysis*. Pergamon Press, Oxford.
Love, A. E. H. (1944). *A Treatise on the Mathematical Theory of Elasticity*. Dover, New York.
Natori, M. and Miura, K. (1985). Deployable structures for space applications. *Proc. 26th Structures, Structural Dynamics and Material Conference*, 1–9.
Pestel, E. C. and Leckie, F. A. (1963). *Matrix Methods in Elastomechanics*. McGraw-Hill, Maidenhead.
Rankin, C. C. and Brogan, F. A. (1984). An element independent corotational procedure for the treatment of large rotations. In *Collapse Analysis of Structures* (Edited by L. H. Sobel and K. Thomas), pp. 85–115. ASME, New York.
Riks, E. (1979). An incremental approach to the solutions of snapping and buckling problem. *Int. J. Solids Structures* **15**(7), 529–551.
Simo, J. C. (1985). A finite strain beam formulation. The three dimensional dynamic problem—Part I. *Comput. Meths Appl. Mech. Engng* **49**, 55–70.
Simo, J. C. and Vu-Quoc, L. (1986). A three-dimensional finite strain rod model—Part II: computational aspects. *Comput. Meths Appl. Mech. Engng* **58**, 79–116.
Thompson, J. M. T. and Hunt, G. W. (1984). *Elastic Instability Phenomena*, pp. 188–194. John Wiley, New York.
Timoshenko, S. P. and Goodier, J. N. (1970). *Theory of Elasticity*, pp. 291–353. McGraw-Hill, Maidenhead.

## APPENDIX: DERIVATIVES OF THE COMPONENTS OF THE STATE VECTOR

1. *First order derivatives* $\{Q_j^{(1)}\}$

(a) *Displacement* $(1 \leqslant j \leqslant 3)$.

$$\mathrm{d}^t\{u_0, v_0, w_0\}/\mathrm{d}z = {}^t\{(1+\varepsilon_0)l_{zx}, (1+\varepsilon_0)l_{zy}, (1+\varepsilon_0)l_{zz}-1\} \tag{A1}$$

where

$$\varepsilon_0 = (l_{zx}\bar{F}_x + l_{zy}\bar{F}_y + l_{zz}\bar{F}_z)/EA. \tag{A2}$$

(b) *Directional cosine* $(4 \leqslant j \leqslant 12)$.

$$\mathrm{d}[l_{ab}]/\mathrm{d}z = [D][l_{ab}]. \tag{A3}$$

(c) *Force and moment* $(13 \leqslant j \leqslant 18)$.

$$\bar{F}_x' = 0, \quad \bar{F}_y' = 0, \quad \bar{F}_z' = 0 \tag{A4a-c}$$

$$\begin{aligned}
\bar{M}_x' &= (l_{zx}l_{yy} - l_{zy}l_{yx})\bar{F}_x + (l_{yy}l_{zz} - l_{zy}l_{yz})\bar{F}_z \\
\bar{M}_y' &= (l_{zx}l_{yy} - l_{zy}l_{yx})\bar{F}_y + (l_{zx}l_{yz} - l_{yx}l_{zz})\bar{F}_z \\
\bar{M}_z' &= (l_{zz}l_{yx} - l_{zx}l_{yz})\bar{F}_x + (l_{zz}l_{yy} - l_{yz}l_{zy})\bar{F}_y.
\end{aligned} \tag{A5a-c}$$

2. *Second order derivatives* $\{Q_j^{(2)}\}$

(a) *Displacement* $(1 \leqslant j \leqslant 3)$.

$$\begin{aligned}
u_0'' &= \varepsilon_0' l_{zx} - (1+\varepsilon_0)(M_x l_{zx}/EI_x + M_y l_{yx}/EI_y) \\
v_0'' &= \varepsilon_0' l_{zy} - (1+\varepsilon_0)(M_x l_{zy}/EI_x + M_y l_{yy}/EI_y) \\
w_0'' &= \varepsilon_0' l_{zz} - (1+\varepsilon_0)(M_x l_{zz}/EI_x + M_y l_{yz}/EI_y)
\end{aligned} \tag{A6a-c}$$

where

$$\varepsilon_0' = -\{(l_{yx}\bar{F}_x + l_{yy}\bar{F}_y + l_{yz}\bar{F}_z)M_y/EI_y + (l_{zx}\bar{F}_x + l_{zy}\bar{F}_y + l_{zz}\bar{F}_z)M_x/EI_x\}/EA \tag{A7}$$

$${}^t\{M_y, -M_x, M_z\} = [l_{ab}]^t\{\bar{M}_y, -\bar{M}_x, \bar{M}_z\}. \tag{A8}$$

(b) *Directional cosine* $(4 \leqslant j \leqslant 12)$.

$$[l_{ab}]'' = [D]'[l_{ab}] + [D][D][l_{ab}]. \tag{A9}$$

Non-zero components of $[D]'$ are given by

$$\begin{aligned}
D'_{12} &= -D'_{21} = (1/EI_y - 1/EI_x)M_x M_y/GJ \\
D'_{13} &= -D'_{31} = \{l_{zx}\bar{F}_x + l_{zy}\bar{F}_y + l_{zz}\bar{F}_z + (1/GJ - 1/EI_y)M_y M_z\}/EI_x \\
D'_{23} &= -D'_{32} = \{l_{yx}\bar{F}_x + l_{yy}\bar{F}_y + l_{yz}\bar{F}_z - (1/GJ - 1/EI_x)M_x M_z\}/EI_y.
\end{aligned} \tag{A10a-c}$$

(c) *Force and moment* $(13 \leqslant j \leqslant 18)$.

$$\bar{F}_x'' = 0, \quad \bar{F}_y'' = 0, \quad \bar{F}_z'' = 0 \tag{A11a-c}$$

$$\begin{aligned}
\bar{M}_x'' &= \{(l_{zx}l_{yy} - l_{zy}l_{yx})M_x/EI_x + (l_{zy}l_{yx} - l_{zx}l_{yy})M_y/EI_y\}\bar{F}_x + \{(l_{yy}l_{zz} - l_{yz}l_{zy})M_x/EI_x + (l_{zy}l_{yz} - l_{yy}l_{zz})M_y/EI_y\}\bar{F}_z \\
\bar{M}_y'' &= \{(l_{yy}l_{zx} - l_{zy}l_{yx})M_x/EI_x + (l_{yx}l_{zy} - l_{zx}l_{yy})M_y/EI_y\}\bar{F}_y + \{(l_{zx}l_{yz} - l_{zz}l_{yx})M_x/EI_x + (l_{zz}l_{yx} - l_{zx}l_{yz})M_y/EI_y\}\bar{F}_z \\
\bar{M}_z'' &= \{(l_{zz}l_{yx} - l_{zx}l_{yz})M_x/EI_x + (l_{zx}l_{yz} - l_{zz}l_{yx})M_y/EI_y\}\bar{F}_x + \{(l_{zz}l_{yy} - l_{zy}l_{yz})M_x/EI_x + (l_{zy}l_{yz} - l_{zz}l_{yy})M_y/EI_y\}\bar{F}_y
\end{aligned} \tag{A12a-c}$$

where

$${}^t\{M_y, -M_x, M_z\} = [l_{ab}]^t\{\bar{M}_y, -\bar{M}_x, \bar{M}_z\}. \tag{A13}$$